Single-mode single-polarization holey fiber using anisotropic fundamental space-filling mode

Masashi Eguchi[1,3] and Yasuhide Tsuji[2,4]

[1]*Department of Applied Photonics System Technology, Chitose Institute of Science and Technology, Chitose 066-8655, Japan*

[2]*Department of Electric and Electronic Engineering, Kitami Institute of Technology, Kitami 090-8507, Japan*

[3]*Corresponding author: megu@mail.gootech.co.jp*

[4]*tsujiya@mail.kitami-it.ac.jp*

Received March 30, 2007; revised May 28, 2007; accepted May 31, 2007; posted June 14, 2007 (Doc. ID 81633); published July 20, 2007

We present the single-mode single-polarization regime of a circular-hole holey fiber consisting of a core with large elliptical holes. The elliptical holes in the core, which produce large anisotropies, split the fundamental mode into two orthogonally polarized fundamental modes, often referred to as slow and fast modes. This fiber can guide only one polarization state of the fundamental mode when a fundamental space-filling mode index of the cladding region is designed to lie between these indices of the slow and fast modes of the core region. We demonstrate one design example of this fiber and show that the single-polarization regime can be achieved over a wide wavelength range. © 2007 Optical Society of America

OCIS codes: 060.2310, 060.2400, 060.2420, 060.2430.

A holey fiber (HF) that guides by total internal reflection is a photonic crystal fiber [1] consisting of a homogeneous medium with a regular lattice of air holes. Owing to their high index contrast, photonic crystal fibers provide a variety of attractive and unique guiding properties, including anomalous waveguide dispersion at short wavelengths [2,3], large mode area [4], high nonlinearity [5,6], endlessly single-mode behavior [7], and high birefringence [8,9]. In HFs consisting of a hexagonal arrangement of holes, birefringence can be produced by breaking the sixfold symmetry [10] of the fiber, which supports the degeneracy of two fundamental modes. Elliptical holes are effective to break the symmetry, and various birefringent HFs using elliptical holes have been proposed [11–14]. Additionally, the systematic investigations of the birefringence of elliptical-hole HFs having a core consisting of multiple defects have recently been reported [15]. In this Letter the realization of single-mode single-polarization HFs using the difference between the fundamental space-filling mode (FSM) [7] for circular-hole lattices and the anisotropic FSM for elliptical-hole lattices is demonstrated by using a numerical simulation [15,16].

To break the sixfold symmetry, we introduce large elliptical holes in the core region of a circular-hole HF. The elliptical-hole core region behaves as an anisotropic medium. The schematic design of our HFs is indicated in Fig. 1. The HF in Fig. 1 represents an elliptical-hole core circular-hole HF (EC–CHF) and is characterized by a lattice pitch Λ, a circular hole size $\xi=d_c/\Lambda$, an elliptical hole size $\xi_e=d_y/\Lambda=0.9$, and an ellipticity $\eta=d_y/d_x=2.0$. The refractive index of fused silica is 1.45. In this fiber, the slow and fast modes correspond to the HE_{11}^y and HE_{11}^x modes, respectively. The FSMs for circular- and elliptical-hole lattices can be controlled by changing the hole size and ellipticity. Figure 2 shows the effective indices n_{eff} of the FSM for several circular-hole lattices ($\xi=0.61, 0.63, 0.65, 0.67$) and an elliptical-hole lattice ($\xi_e=0.9$ and $\eta=2.0$). Here, Λ/λ is the normalized frequency. In Fig. 2, the solid and dashed curves denote the FSMs for the circular holes and the two orthogonally polarized FSMs for the elliptical holes, respectively. In HFs, the FSM provides the cutoff of the guided mode in the infinite hole lattice. When the FSM of the cladding region is designed to lie between those of the slow (FSM_e^y) and fast (FSM_e^x) modes of the core region consisting of elliptical holes, the HF can guide only one polarization state. In Fig. 2, this condition is satisfied when the solid curve lies between the two dashed curves corresponding to the slow and fast FSMs of the elliptical-hole lattice.

Figure 3 shows the circular hole sizes (shaded region) satisfying this design condition. The permissible range of circular hole sizes expands as Λ/λ decreases. This is because the FSM birefringence of the elliptical hole increases with wavelength. This range also depends on the ellipticity and size of elliptical holes. In the permissible range, the FSM of the circular hole lies between the two polarized FSMs for the elliptical hole. The fundamental mode in the EC-CHF

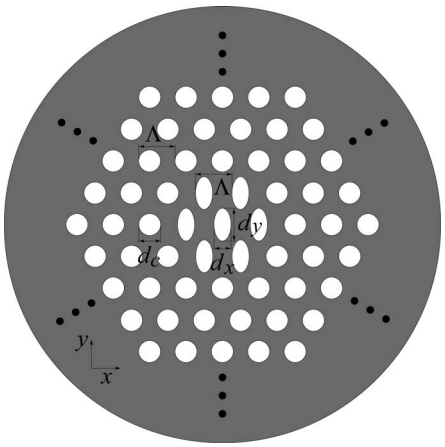

Fig. 1. Circular-hole HF having a core consisting of elliptical holes.

0146-9592/07/152112-3/$15.00

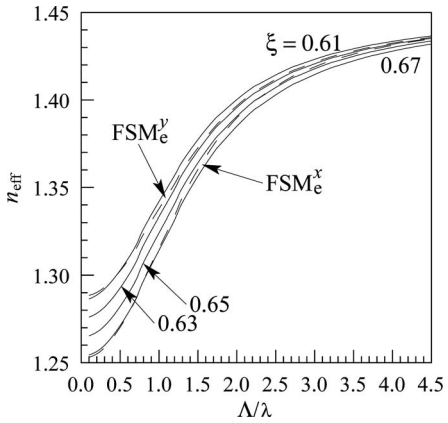

Fig. 2. Effective index n_{eff} of the FSMs for circular- (solid curves) and elliptical-hole (dashed curves) lattices against the normalized frequency Λ/λ. FSM_e^y and FSM_e^x correspond to the slow and fast FSMs of elliptical-hole lattice, respectively.

lies between the FSMs for the circular- and elliptical-hole lattices. This is because the two orthogonally polarized FSMs for the elliptical-hole lattice are converted to the slow and fast guided modes in the EC-CHF when elliptical holes in the core surround are replaced by circular holes. Moreover, the two polarized modes coincide with the FSM for the circular-hole lattice, if all elliptical holes are replaced by circular holes. Figures 4(a) and 4(b) show the intensity distributions of the slow mode for the single-polarization EC-CHF ($\xi=0.63$) at $\Lambda/\lambda=4.6$ and $\Lambda/\lambda=0.8$, respectively. The guided mode at $\Lambda/\lambda=4.6$ is not affected by the average index of the core, whereas the mode field at $\Lambda/\lambda=0.8$ is confined to the core region. In addition, circular hole sizes ξ should be expanded to achieve a better confinement of light. Cutoff of the first higher-order mode is another important characteristic of single-mode single-polarization fibers. In Fig. 3, the normalized cutoff frequency of EC-CHF against the circular hole size ξ of cladding is also indicated by the dashed-dotted curve.

An example is shown in Fig. 5 for an EC-CHF with $\xi=0.65$, $\xi_e=0.9$, and $\eta=2.0$. The cutoff frequency is indicated on the horizontal axis by an arrow. For the EC-CHF, the first higher-order mode corresponds to the HE_{21}^y mode. In Fig. 5, the thick, thin, and dashed curves correspond to the single-polarization fundamental mode, the FSM for the cladding region, and the two polarized FSMs for the core region, respectively. This EC-CHF can guide only one polarization state over a wide wavelength range. Additionally, the single-mode single-polarization regime can be achieved in the frequency range to the left of the arrow ($[\Lambda/\lambda]_c=1.16$). Figure 6 shows the intensity distribution of the slow mode at $\Lambda/\lambda=0.8$. Although the mode field has a central dip, it is well confined and is relatively comparable with those of standard fibers. For silica [17], the calculated chromatic dispersion of this example is illustrated in Fig. 7, where a lattice constant of $\Lambda=1$ μm is assumed. In Fig. 7, the solid and dashed curves denote total D_T and material D_M dispersions, respectively. The total dispersion is given by

$$D_T = -\frac{\lambda}{c}\frac{d^2 n_{\text{eff}}}{d\lambda^2}, \tag{1}$$

where c is the velocity of light. Since this example is not designed to have optimum dispersion properties,

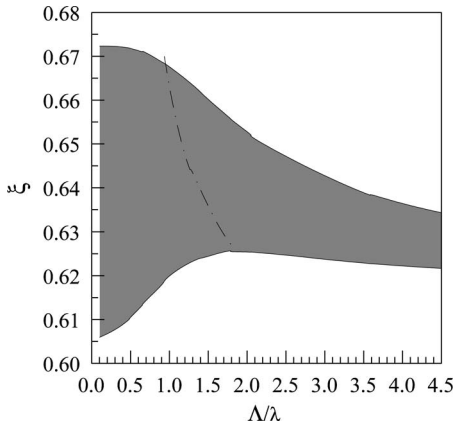

Fig. 3. Permissible range of circular hole sizes satisfying only one polarization state against the normalized frequency. The dashed–dotted curve indicates the normalized cutoff frequency of EC-CHF.

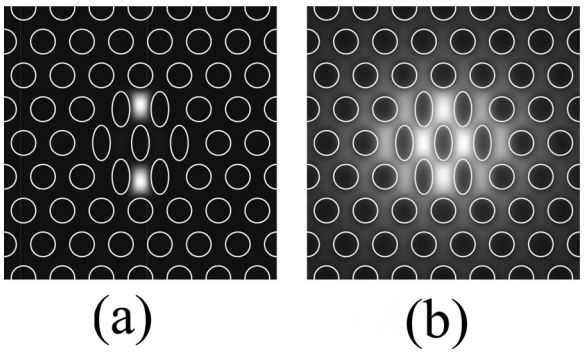

Fig. 4. Intensity distributions of the slow mode for an EC-CHF with $\xi=0.63$ at (a) $\Lambda/\lambda=4.6$ and (b) $\Lambda/\lambda=0.8$.

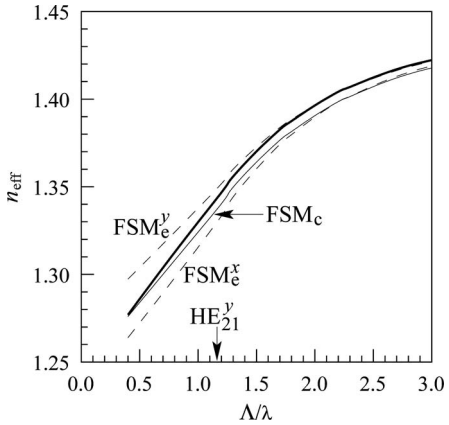

Fig. 5. Dispersion properties of the single-polarization fundamental mode (thick curve), the FSM (thin curve) for the cladding region, and the two polarized FSMs (dashed curves) for the core region in an EC-CHF with $\xi=0.65$. FSM_e^y and FSM_e^x correspond to the slow and fast FSMs of elliptical-hole lattice, respectively. The cutoff frequency is indicated on the horizontal axis by an arrow.

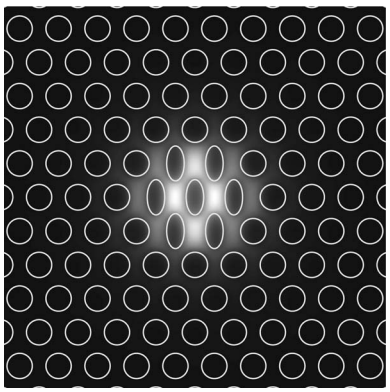

Fig. 6. Intensity distributions of the slow mode for an EC-CHF with $\xi=0.65$ at $\Lambda/\lambda=0.8$.

it has large total dispersion associated with the large waveguide dispersion of a HF having large air holes. The total dispersion can be easily controlled by changing air hole sizes. These optimum dispersion designs will be investigated in the future. Its dispersion slope changes from negative to positive with increasing wavelength. As mentioned above, the reason for this is that in the short wavelength range a guided mode is not affected by the average index of the core consisting of elliptical holes. In this case, the cutoff wavelength is $\lambda_c=1.0/1.16\simeq 0.862\ \mu$m and is indicated by an arrow. On the other hand, the single-mode single-polarization transmission can be realized at wavelength of 1.55 μm by using the lattice constant of $\Lambda<[\Lambda/\lambda]_c\times 1.55=1.798\ \mu$m.

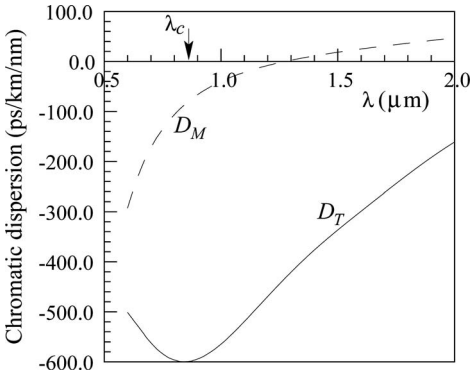

Fig. 7. Chromatic dispersion for an EC-CHF of Fig. 5. Solid curve, total dispersion D_T. Dashed curve, material dispersion D_M. The cutoff wavelength λ_c is indicated by an arrow.

In conclusion, we have demonstrated a single-mode single-polarization HF by using the anisotropic FSM of elliptical-hole lattices. The single-polarization regime can be easily achieved only by the design of the FSMs for circular- and elliptical-hole lattices. Our calculations indicate that the EC-CHF can guide only one polarization state of the fundamental mode.

References

1. J. C. Knight, T. A. Birks, P. St. J. Russell, and D. M. Atkin, Opt. Lett. **21**, 1547 (1996).
2. M. Gander, R. McBirde, J. Jones, D. Mogilevtsev, T. Birks, J. Knight, and P. Russell, Electron. Lett. **35**, 63 (1999).
3. J. C. Knight, J. Arriaga, T. A. Birks, A. Ortigosa-Blanch, W. J. Wadsworth, and P. St. J. Russell, IEEE Photon. Technol. Lett. **12**, 807 (2000).
4. J. C. Knight, T. A. Birks, R. F. Cregan, P. St. J. Russell, and J.-P. De Sandro, Electron. Lett. **34**, 1347 (1998).
5. J. K. Ranka, R. S. Windeler, and A. J. Stentz, Opt. Lett. **25**, 796 (2000).
6. P. Petropoulos, T. M. Monro, W. Belardi, K. Furusawa, J. H. Lee, and D. J. Richardson, Opt. Lett. **26**, 1233 (2001).
7. T. A. Birks, J. C. Knight, and P. St. J. Russell, Opt. Lett. **22**, 961 (1997).
8. K. Suzuki, H. Kubota, S. Kawanishi, M. Tanaka, and M. Fujita, Opt. Express **9**, 676 (2001).
9. T. P. Hansen, J. Broeng, S. E. B. Libori, E. Knudsen, A. Bjarklev, J. R. Jensen, and H. Simonsen, IEEE Photon. Technol. Lett. **13**, 588 (2001).
10. M. J. Steel, T. P. White, C. M. de Sterke, R. C. McPhedran, and L. C. Botten, Opt. Lett. **26**, 488 (2001).
11. M. J. Steel and R. M. Osgood, Jr., Opt. Lett. **26**, 229 (2001).
12. M. J. Steel and R. M. Osgood, Jr., J. Lightwave Technol. **19**, 495 (2001).
13. W. Belardi, G. Bouwmans, L. Provino, and M. Douay, IEEE J. Quantum Electron. **41**, 1558 (2005).
14. D. Chen and L. Shen, IEEE Photon. Technol. Lett. **19**, 185 (2007).
15. M. Eguchi and Y. Tsuji, J. Opt. Soc. Am. B **24**, 750 (2007).
16. Z. Zhu and T. G. Brown, Opt. Express **10**, 853 (2002).
17. I. H. Malitson, J. Opt. Soc. Am. **55**, 1205 (1965).